Macromolecules

ARTICLE

pubs.acs.org/Macromolecules

Molecular Simulations of PIM-1-like Polymers of Intrinsic Microporosity

Gregory S. Larsen,[†] Ping Lin,[‡] Kyle E. Hart,[†] and Coray M. Colina*[,†]

[†]Department of Materials Science and Engineering and [‡]Materials Simulation Center, The Pennsylvania State University, University Park, Pennsylvania 16802, United States

Supporting Information

ABSTRACT: Polymers of intrinsic microporosity, or PIMs, are characterized by rigid and nonlinear or nonplanar backbones that inhibit space efficient packing, thus creating microporosity. PIM-1 has been well studied by both simulations and experiments and is compared in this work to two different PIM-1-like polymers, PIM-1c and PIM-1n. A detailed method for the generation of representative structures, including charge assignment from *ab initio* calculations, is presented along with simulated characterization of the pore size distributions, surface areas, structure factors, and methane adsorption isotherms. Simulated scattering for PIM-1c and PIM-1n show similar characteristic peaks as PIM-1, suggesting similar conformations. Adsorption isotherms of methane in PIM-1, PIM-1c, and PIM-1n were also predicted and compared to experimental data for PIM-1.

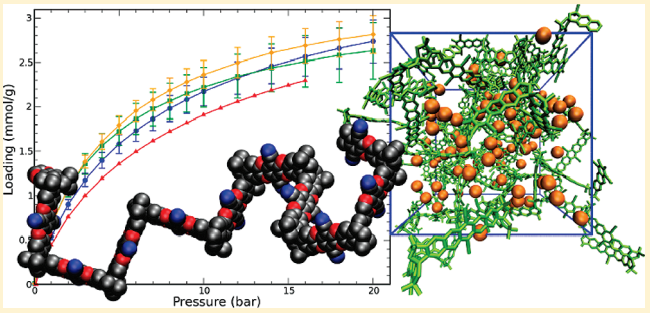

INTRODUCTION

Gas adsorption is an important process with many applications, including gas storage and separations. As necessity to use energy efficient and environmentally friendly processes increases, so too do the requisites for the design and development of tailor-made adsorbent materials. While all solids are capable of adsorption, the vast majority lack sufficient capacity and selectivity for practical use. An ideal material for adsorption and separations will have a combination of micropores (size less than 2 nm) to give high capacity/selectivity and meso- or macropores (between 2 and 50 nm and larger than 50 nm, respectively) to give fast sorption kinetics (pore sizes named according to IUPAC convention[1,2]).

To date, a wide range of microporous materials have been investigated. Two broad classes of materials are crystalline and amorphous materials typified by activated carbons and zeolites.[2,3] Because of the low costs, high surface areas, and large sorption capacities, activated carbons are widely used in industry. Zeolites can occur naturally or be synthesized and are commonly used in kinetic separations and catalysis. Chemically, the different zeolites are very similar, typically aluminosilicates or aluminophosphates, but vary widely in pore topology. Of more recent interest, metal organic frameworks[4] (MOFs), as well as porous organic frameworks, porous coordination polymers, etc., consist (usually) of metal ligands separated by rigid organic linkers. By varying the ligand and/or linkers, a large number of structures can be made. MOFs have been demonstrated to have extremely high surface areas exceeding 6000 $m^2\ g^{-1}$. Snurr and co-workers have used molecular simulations extensively to screen novel MOF architectures and enhance understanding of the adsorption process.[5,6] For a complete reviews of microporous materials the reader is referred, e.g., to refs 2 and 3 and references therein.

The lightweight organic constituents, functionalizability, and potential for industrial scaling are making polymers attractive as potential microporous materials. However, the generally flexible nature of polymers allows for space efficient packing with almost no micropores and hence poor material properties for storage and separations. To date, several porous polymers have been created.[7] One example, hyper-cross-linked polymers, are made by extensive cross-linking of a swollen polymer using rigid cross-linkers such that the microporosity is generally maintained after solvent removal. Various groups have used a combination of simulations and experiments to investigate these materials.[8−10]

Polymers of intrinsic microporosity (PIMs) represent a novel class of porous materials that derive their porosity not from processing conditions, but from their unique molecular structure, which inhibits space efficient packing.[11] By creating monomers that are both rigid and nonlinear or nonplanar, the resulting polymeric material develops a microporous structure. PIMs with surface areas in excess of 1000 $m^2\ g^{-1}$ of BET surface area have been recently synthesized.[12] PIMs have shown hydrogen uptakes as high as 1.83 wt % at 0.1 MPa and 77 K[12] and are pushing the Robeson upper bound of permeability and selectivity.[13]

Molecular simulations represent a powerful and widely used tool for the investigation and study of adsorbent materials. Classical molecular dynamics (MD) and Monte Carlo (MC)

Received: February 14, 2011
Revised: June 14, 2011
Published: August 03, 2011

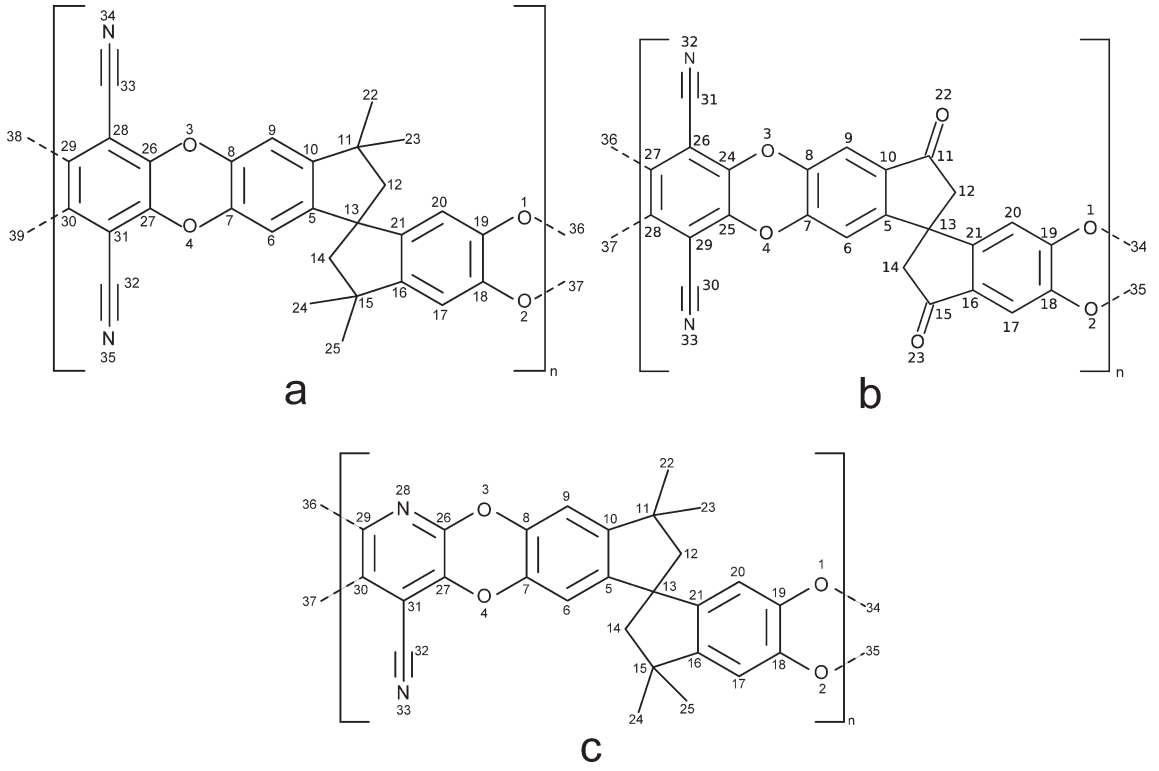

Figure 1. Chemical structure of (a) PIM-1, (b) PIM-1c, and (c) PIM-1n. Numbers correspond to atoms for simulation parameters listed in Table 1.

simulations are particularly well suited to the study of physical adsorption because the phenomenon depends primarily on van der Waals and electrostatic interactions between the sorbent and the sorbate. While experiments provide physical data, they are often hindered by limitations in the equipment, sample quality, and interpretive models. Molecular simulations can help by looking at ideal systems as well as experimentally inaccessible conditions and by providing a high level of detail (often atomistic). Simulations can be used not only to study adsorption but also to calculate key materials properties such as pore size distributions, surface areas, structure factors, enthalpies of adsorption, and selectivities of gas mixtures. Once validated against experimental data for known materials, simulations can be applied as virtual experiments to screen conceptualized materials.

The aim of this research is to aid in the rational design of novel PIMs for application in gas storage and separations. The work presented here focuses on the preparation, characterization, and adsorption capabilities of a realistic simulation sample of PIM-1 and two bifunctional polymers, in this work called PIM-1c and PIM-1n. Both PIM-1c[14] and PIM-1n[15] have been recently synthesized. PIM-1 is the prototypical example of PIMs and has been extensively studied from an experimental point of view. PIM-1c and PIM-1n were chosen because they represent small and controlled changes to the PIM-1 structure that have been synthesized; however, to date, minimal experimental characterization data exist for these polymers. The similarities between the three samples allow for the effects of a single functional change on the material's characteristics and properties to be isolated, while the feasibility of synthesizing them will allow for experimental verification. In this work, methane was chosen as the adsorbate for both its simplicity and to isolate the effects of the conformational alterations from electronic changes of the materials by adsorbing neutral species.

SAMPLE GENERATION

The generation of a realistic simulation sample for amorphous materials is still a challenge. For crystalline materials, various diffraction techniques can be used to experimentally derive the structure of the unit cell. These structures are an invaluable starting point for simulations and are unavailable for amorphous materials such as PIMs. The so-called reconstruction techniques attempt to create simulation samples that reproduce a given set of experimental data.[16] For polymeric materials, the method of Theodorou and Sutter[17] is widely used, even for PIM-like structures.[18−20] Other complex amorphous materials, such as activated carbons and porous glasses, often use a reverse Monte Carlo (RMC) technique, in which additional MC criteria are used to guide the sample structure generation toward reproducing some experimental data, such as structure factors or correlation functions.[21−24]

In the case of PIMs the creation of the packing model, especially one that accurately represents the material, is nontrivial. The chemical structure of the repeat units of PIM-1, PIM-1c, and PIM-1n are shown in Figure 1; the spirocenter at the junction of the two five-membered rings can create a nearly right angle bend into or out of the page, resulting in two distinct chiralities. In this work, chains are randomly initiated throughout the cubic simulation box of length L and grown in a stepwise manner by randomly choosing one of the two chiralities and one of the two possible orientations, until the target chain length is achieved or an overlap results from any further growth. Ultimately, the growth stage is completed when a target density is achieved. The system is grown at a low density, ~0.07 g cm^{-3}, similar to other simulations of glassy polymers that contain aromatic moieties.[20,25,26] This procedure allows chains to grow without hard core overlaps.

Table 1. Nonbonded Interaction Parameters for the Simulations of PIM-1, PIM-1c, and PIM-1n[a]

				PIM-1		PIM-1c		PIM-1n	
atom type	ref	ε (K)	σ (Å)	number	charge (eV)	number	charge (eV)	number	nharge (eV)
C(aro)−O(aro)−X(aro)	31	70	2.6	1, 2, 3, 4	−0.219 064	1, 2, 3, 4	−0.108 096	1, 3	−0.195 57
								2, 4	−0.122 86
X(aro)−C(aro)−X(aro)	30	30.7	3.6	7, 8, 18, 19	0.177 839	7, 8, 18, 19	−0.193 873	7, 18	−0.216 376
				26, 27, 29, 30	0.172 261	24, 25, 27, 28	0.319 062	8, 19	−0.187 905
				36, 37	0.0	34, 35	0	26, 29	0.613 545
								27, 30	0.235 411
								34, 35	0
R−C(aro)	32	21	3.88	5, 10, 16, 21	0.038 356	5, 10, 16, 21	−0.131 754	5, 16	−0.117 238
				28, 31	−0.123 04	26, 29	−0.376 824	10, 21	−0.142 221
								31	−0.332 763
CH(aro)	32	50.5	3.695	6, 9, 17, 20	−0.124 962	6, 9, 17, 20	0.318 224	6, 17	0.289 326
								9, 20	0.302 41
C	33	0.5	6.4	11, 13, 15	0.097 945 4	13	0	11,13, 15	0
CH_2	34	51	3.89	12, 14	−0.016 466	12, 14	0.192 322	12, 14	0.117 757
CH_3	28, 32	98	3.75	22, 23, 24, 25, 38, 39	0.0	36, 37	0	22, 23, 24, 25, 36, 37	0
C(sp, nitrile)	32	60	3.55	32, 33	0.313 718	30,31	0.302 473	32	0.320 622
N(nitrile)	32	60	2.95	35, 35	−0.409 99	32, 33	−0.368 858	33	−0.381 284
C(sp^2, ketone)	35	40	3.82			11, 15	0.314 104		
O(ketone)	34	79	3.05			22, 23	−0.470 344		
C(aro)−N(aro)−X(aro)	31	57	3.2					28	−0.759 13

[a] Lennard-Jones parameters are taken from the TraPPE potential. Charges are from *ab initio* calculations performed in this work. Atom numbers correspond to the respective chemical structures shown in Figure 1a.

Table 2. 12-Step and Slow Decompression MD Compression and Relaxation Schemes[a]

step	12-step conditions	duration (ps)	step	slow decompression conditions	duration (ps)
1	NVT 600 K	50	1	NVT 600 K	50
2	NVT 300 K	50	2	NVT 300 K	50
3	NPT 0.2P_{max} bar, 300 K	50	3	NPT 0.02P_{max} bar, 300 K	50
4, 5	NVT 600 K, NVT 300 K	50, 100	4, 5	NVT 600 K, NVT 300 K	50, 100
6	NPT 0.6P_{max} bar, 300 K	50	6	NPT 0.6P_{max} bar, 300 K	50
7,8	NVT 600 K, NVT 300 K	50, 100	7, 8	NVT 600 K, NVT 300 K	50, 100
9	NPT P_{max} bar, 300 K	50	9	NPT P_{max} bar, 300 K	50
10, 11	NVT 600 K, NVT 300 K	50, 100	10, 11	NVT 600 K, NVT 300 K	50, 100
12	NPT 1 bar, 300 K	800	12	NPT 0.5P_{max} bar, 300 K	5
			13, 14	NVT 600 K, NVT 300 K	5, 10
			15	NPT 0.1P_{max} bar, 300 K	5
			16, 17	NVT 600 K, NVT 300 K	5, 10
			18	NPT 0.01P_{max} bar, 300 K	5
			19, 20	NVT 600 K, NVT 300 K	5, 10
			21	NPT 1 bar, 300 K	800

[a] P_{max} was varied to determine the effect on the final system density (see Figure 2).

While it is common practice in molecular simulations of polymers to use a single long chain to reduce the effects of chain ends, the rigid and awkward structure of PIMs makes this impractical. Thus, chain growth was generally terminated after 10 monomers were added or an overlap resulted from any further additions, as in previous work,[20] resulting in samples of approximately 10−15 chains in the simulation box. Charge-neutral steric blocking groups were added to the chain ends to eliminate any high-energy sites and reduce the effect of the higher chain end density in the simulations.

The low-density initial structure, described above, is transformed by a series of short MD simulations into a sample of realistic density. MD simulations are performed using LAMMPS[27] with the Nosé-Hoover thermostat and barostat. As there are no hydrogen atoms capable of hydrogen bonding present in the PIMs studied in this work, the polymers are described here using a united atom (UA) representation. Nonbonded interaction parameters are taken from the TraPPE potential[28] and charges from *ab initio* calculations performed in this work. Bonded interaction parameters, as suggested by the TraPPE potential, are

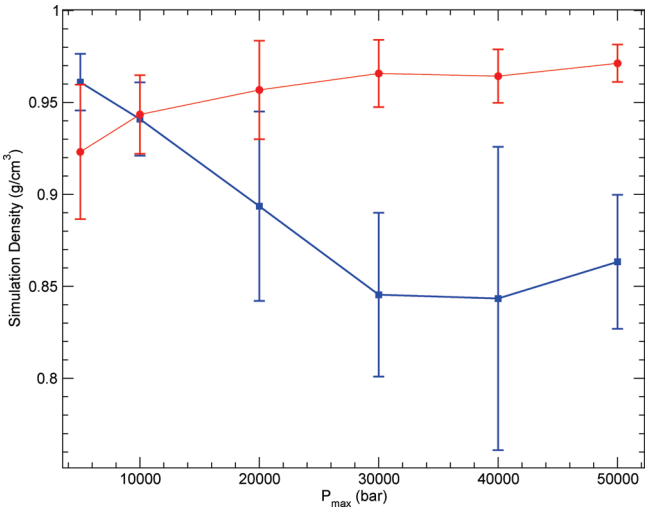

Figure 2. Final PIM-1 simulation density as a function of the maximum pressure for the single iteration 12-step (■) and slow decompression (●) schemes. The results shown represent averages of at least five unique samples for each data point. Error bars represents standard deviations.

obtained from the GAFF[29] force field. Because of the highly delocalized electron structure of the polymer, we elected to use charges from *ab initio* calculations. Charges were determined similar to previous work[20] using calculations for monomer models in the gas phase at the HF/6-31G* level of theory followed by a restrained electrostatic potential (RESP)[30] charge fitting with multiple configurations. All nonbonded interactions parameters used in this work are listed in Table 1.

Two previously suggested schemes to compress and relax the polymer samples were explored and modified. The work of Hofmann et al.,[25] here referred to as the 12-step scheme and outlined in Table 2, was originally applied successively until a consistent density was achieved. Later, Karayannis et al.[26] extended the 12-step scheme successively to include annealing and decompression. Here, we develop a new generic scheme based on that of Karayannis et al.; this so-called 21-step compression/relaxation scheme, outlined in Table 2, consistently compresses and relaxes PIM samples to experimental densities and configurations.

In Figure 2, the results are compared for the slow decompression and a single iteration of the 12-step scheme as a function of maximum pressure for PIM-1. The 21-step slow decompression scheme provides final simulation densities which are independent of the maximum pressure, whereas the 12-step scheme has a tendency to give lower and less consistent final densities with increasing maximum pressure. The inconsistency of the 12-step scheme, particularly at higher maximum pressures, is likely due to the dramatic release of pressure allowing for an uncontrolled decompression. It is important to note that Hoffmann et al.[25] used a trial and error process, repeating the 12-step scheme as many times as necessary, until obtaining a density consistent with available experimental data. The slow decompression scheme used in this work is advantageous since its provides consistent densities independent of the maximum pressure selected and thus avoids both a trial and error process to obtain the desired target density and the necessity for experimental data with which to compare. Maximum temperatures up to 1800 K were studied with both schemes, and the results (not shown) are independent of the maximum temperature selected. Here, we use the slow decompression scheme with a maximum temperature of 600 K and maximum pressure of 50 000 bar.

Experimentally, the skeletal volume is measured, while in molecular simulations the total box volume is considered. Thus, the simulated density differs from the experimentally measured skeletal density by the pore volume per unit mass according to[20]

$$\frac{1}{\rho_{sim}} = \frac{1}{\rho_{exp}} + \frac{v_{pore}}{m} \quad (1)$$

where ρ_{sim} is the simulated density, ρ_{exp} is the experimental skeletal density, v_{pore} is the pore volume, and m is the mass of the sample. From simulated helium adsorption, the pore volume can be calculated as[36]

$$v_{pore} = \frac{n_{ads}}{\rho_{He}} \quad (2)$$

where n_{ads} is the amount of helium adsorbed and ρ_{He} is the density of helium at the temperature and pressure of the simulation. In the case of PIM-1 the pore volume was calculated as 0.194 cm^3 g^{-1} such that a simulated density of 0.98 g cm^{-3} corresponds to a skeletal density of ~1.202 g cm^{-3}. Previous works have reported simulated densities of 1.031[18] and 1.07 g cm^{-3} (average of three boxes).[19] Our simulated density agrees well with previous work, and the calculated skeletal density falls within the broad range of experimentally measured values.[19,20,37] Simulation densities of 1.104 and 0.959 g cm^{-3} and pore volumes of 0.159 and 0.220 cm^3 g^{-1} for PIM-1c and PIM-1n correspond, via eq 1, to calculated skeletal densities of 1.34 and 1.22 g cm^{-3}, respectively; however, to our knowledge, no experimental densities have been reported for PIM-1c or PIM-1n.

It is common in simulations to utilize periodic boundary conditions both to ensure the simulation of bulk material properties and maximize the computational efficiency by limiting the number of particles in the system.[38] Amorphous materials, lacking the natural periodicity of a unit cell found in crystalline materials, require the simulation sample to be sufficiently large to include features of the largest length scale of interest observed in the material experimentally. The key feature in a porous material is the size of the pores, which is related to the fractional free volume (FFV). In this work, the torsion parameters used were corrected to half the values previously employed in ref 20 (see Supporting Information). As in previous work,[20] the comparison of FFVs for different size samples was used to determine the optimal box size, and the same conclusions for the optimal box size were reached. In the case of PIM-1, simulations boxes of L = 32, 45, and 55 Å samples were compared. The 32 Å sample showed a wide variability in FFV while the 45 and 55 Å samples were similar, suggesting that the 45 Å sample size provides the smallest yet sufficient size. Additionally, simulated density, surface areas, and scattering were also calculated and consistent at all box sizes, corroborating that FFV is a more sensitive variable for the selection of the box size. In the lack of experimental data, and due to their structural similarities to PIM-1, a sample size of L = 45 Å is assumed to be sufficient for PIM-1c and PIM-1n.

■ VALIDATION AND CHARACTERIZATION

The structure generation scheme described above presents systematic methods and produces samples with densities comparable to experimentally reported values. However, given the broad range of densities reported, an additional verification that the samples accurately describe the materials is needed.

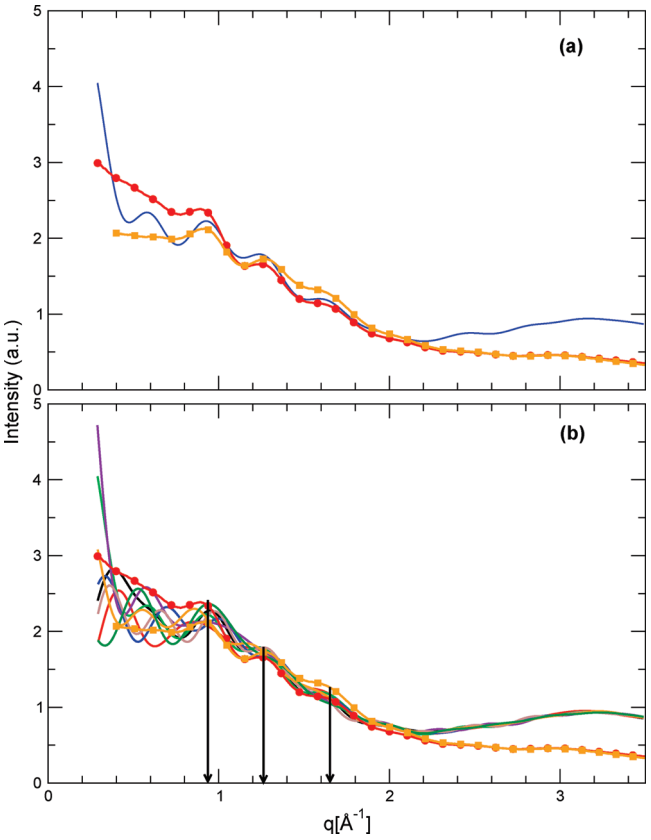

Figure 3. (a) A single representative simulated scattering pattern of PIM-1 (—) which reproduces the slope and characteristic peaks observed experimentally in the methanol-treated film and untreated powder of PIM-1 (● and ■, only every 75th data point is indicated with a symbol).[41] (b) Simulated scattering patterns for multiple simulation samples of PIM-1 are compared to one another (solid lines) and to experimental data of a methanol-treated film (●) and non-methanol-treated powder (■) (only every 75th data point is indicated with a symbol) from ref 41. Greater variation between samples is observed at low q, where length scales are comparable to half the box size; at higher q where length scales are comparable to pore size and chain spacing the samples converge.

This validation may be accomplished by comparing simulated and experimental X-ray scattering data. The X-ray scattering is a better choice of data for sample validation than the PSD because the PSD is experimentally derived normally from adsorption isotherms and thus depends on the models and assumptions used to interpret the data. Calculation of the structure factor from simulation samples is a well-established practice.[39] Simulated scattering was performed using ISAACS[40] with structural data from ten snapshots taken during a 500 ps NVT run at the end of the compression and relaxation scheme described above. The scattering data are calculated from partial radial distribution functions as described elsewhere.[39,40] As this work uses a UA model, a first approximation of the scattering pattern was calculated ignoring contributions from hydrogen. This approximation is justified by both the small mole fraction and scattering length of hydrogen.

Simulated scattering patterns for PIM-1 are compared to experimental WAXS data[41] in Figure 3a,b. Despite the variation at low q, the simulated scattering patterns all reproduce the three characteristic peaks (marked in Figure 3b). The scattering vector q is inversely proportional to distance; thus, the low q values represent longer lengths, and the low q limit is defined by the size

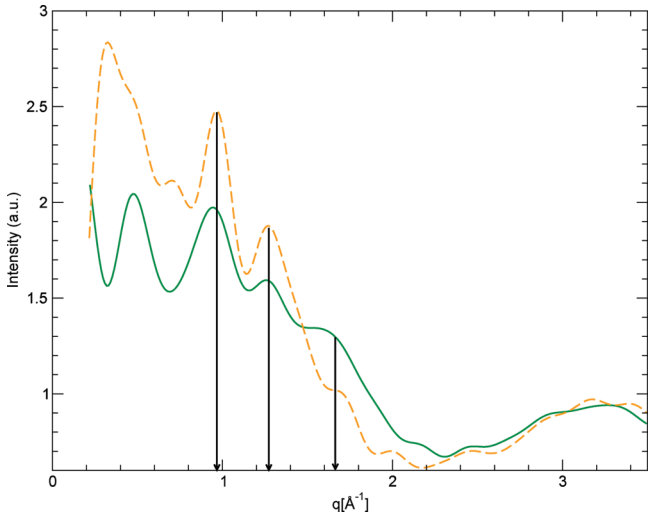

Figure 4. Simulated scattering patterns for PIM-1c (—) and PIM-1n (– –). The predicted patterns of PIM-1c and PIM-1n show similar characteristic peaks to PIM-1, highlighted with arrows.

of the simulation sample. In the low q region, greater variation between samples is observed as an inherent consequence of box size limitations and periodic boundary conditions. At intermediate q values, representative of length scales comparable to pore size and chain spacing, all samples converge and give results consistent with experimental data. At the highest q values, deviations are again observed between the simulations and experiments, here likely due to the assumption of q independent scattering lengths in the simulations. Analysis of the partial structure factors from simulations suggests that the characteristic peaks and the slope on which they are superimposed are indicative of interchain spacing and intersegmental distances.[41] Predicted scattering patterns for representative samples of PIM-1c and PIM-1n are shown in Figure 4.

The good correlation between the simulated and experimental scattering patterns for PIM-1 suggests that the structure generation schemes described above create simulation samples representative of the experimental material and warrant further characterization. We first turn our attention to the PSD which, while critical in understanding the adsorption process at the microscopic level, is difficult to measure experimentally. Two of the most common experimental techniques are the Horvath–Kawazoe (HK) method[42] and positron anihilation lifetime spectroscopy (PALS).[43] In both methods, complex models and assumptions are used to transform the experimental data into a PSD. In comparison, molecular simulations can directly measure the FFV and PSD geometrically with no complex models or assumptions and may therefore be useful in interpreting experimental data. The FFV is used to derive the PSD by differentiation with respect to the pore width:[44]

$$PSD = -\frac{\mathrm{d}FFV}{\mathrm{d}W} \tag{3}$$

PSD's for PIM-1, PIM-1c, and PIM-1n were calculated as in previous work[20] and are compared in Figure 5.

The similar chemical structures of PIM-1, PIM-1c, and PIM-1n produce similar PSDs with peaks at 3.2, 2.5, and 3.2 Å, respectively. Previous simulations have found PIM-1 PSD peaks at 2.2[18] and 6 Å[19]. By comparing the radial distribution functions

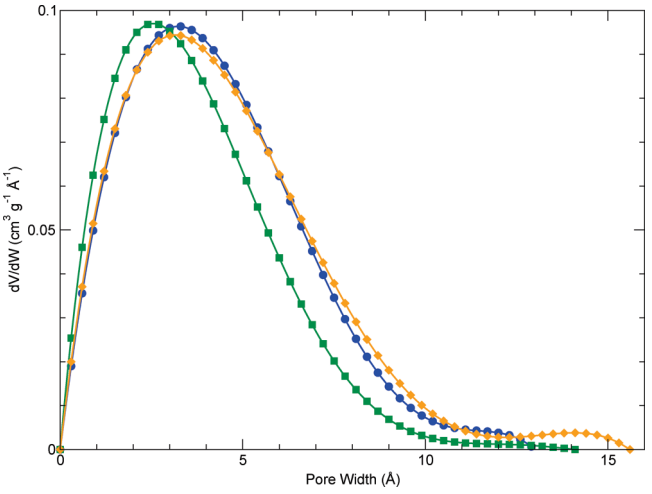

Figure 5. Comparison of the simulated PSD for PIM-1 (●), PIM-1c (■), and PIM-1n (◆). The PSD peak position for PIM-1, PIM-1c, and PIM-1n are at 3.2, 2.5, and 3.2 Å, respectively.

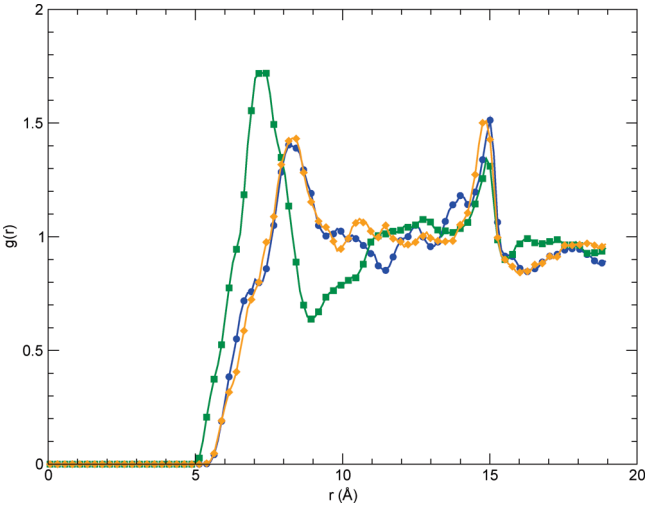

Figure 6. Spirocenter−spirocenter radial distribution function for PIM-1 (●), PIM-1c (■), and PIM-1n (◆) all show a similar pattern. The sharp peak at 15 Å corresponds to the distance between adjacent spirocenters on the same chain. Both PIM-1 and PIM-1n, which have the same spirocenter functionalization, show almost identical RDF peaks at 8.2 Å. PIM-1c, which has a lower volume carbonyl functionalization at the spirocenter, shows a similar pattern with the first peak shifted to smaller distances, implying that the lower volume functionalization at the spirocenter allows the chains to pack closer together.

(RDF) of the spirocenter carbons in each structure (atom number 13 in Figure 1), some insight into the PSD variations can be elucidated. The radial distribution function, $g_{a,b}(r)$, gives the density of b in the shell of inner radius r and outer radius $r + dr$ around any atom a normalized to the bulk density of b.[45] In Figure 6, the spirocenter−spirocenter RDFs for each structure are compared. All samples show a peak at 15 Å which corresponds to the distance between adjacent spirocenters on the same chain. PIM-1 and PIM-1n show nearly identical RDFs while the RDF of PIM-1c is the same shape, but the first peak is shifted to smaller distances. Both PIM-1 and PIM-1n have the same dimethyl functionalization of the spirocenter while PIM-1c has carbonyl oxygens. This suggests that the lower volume carbonyl

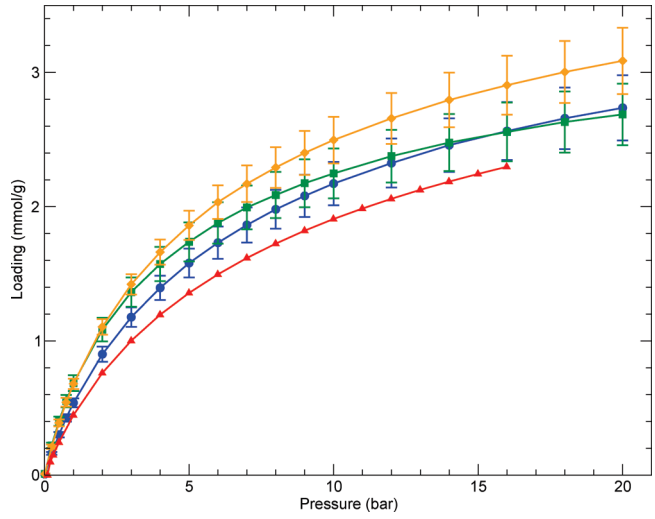

Figure 7. Simulated adsorption isotherms of methane at 20 °C in PIM-1 (●), PIM-1c (■), and PIM-1n (◆) compared with experimental adsorption (▲) of methane in powdered PIM-1 at 20 °C from ref 50.

oxygen functionalization in PIM-1c allows the spirocenters, and therefore the rest of the chain, to pack more closely, which causes the PSD peak to shift to a slightly lower value.

As with the PSD, molecular simulations provide a direct geometric measurement of the surface area while experimental measurements might be hindered by complex models and data analysis. Numerous definitions of surface area can be used, but it has been suggested that the solvent accessible surface area is most appropriate for comparison to BET surface areas.[46] Experimental BET surface areas for PIM-1 have been reported from 750 to 860 m^2 g^{-1} [47−49] and 501 m^2 g^{-1} for PIM-1c.[14] The simulated solvent accessible SA of PIM-1, PIM-1c, and PIM-1n averaged over five samples are calculated as 448.99 ± 85.18, 319.28 ± 116.63, and 479.73 ± 98.47 m^2 g^{-1}, respectively, using a nitrogen size probe of 3.681 Å. The surface area calculated for PIM-1 is similar to the GCMC nitrogen adsorption based calculation of 435 m^2/g from.[19] The simulations correctly predict the surface areas of PIM-1 and PIM-1c relative to one another but give generally lower values. Possible sources of this deviation may include (1) experimental model assumptions, e.g., slit pores or nitrogen interaction parameters, (2) residual solvent or contaminants in the experimental sample, (3) differences in sample histories between simulated and real materials, or (4) kinetically inaccessible pores within the experimental sample.

■ ADSORPTION

The well-equilibrated and realistic simulation samples are subjected to grand canonical Monte Carlo (GCMC) simulations to calculate excess adsorption isotherms. GCMC simulations were performed with the MCCCS Towhee code.[33] The input chemical potentials were calculated according to the ideal gas approximation (which can be considered valid over the temperature and pressure ranges studied in this work)

$$\mu = k_B T \ln\left(\frac{P\Lambda^3}{k_B T}\right) \quad (4)$$

where k_B is Boltzmann's constant, T is the temperature in kelvin, and Λ is the de Broglie wavelength. As experiments measure the

dx.doi.org/10.1021/ma200345v |*Macromolecules* 2011, 44, 6944–6951

excess adsorption, simulation data must be converted from total adsorption according to

$$n_{exc} = n_{tot} - v_{pore}\rho_g \quad (5)$$

where n_{tot} is the total adsorption, v_{pore} is the pore volume as defined above, and ρ_g is the density of the adsorbate gas at the given temperature and pressure. Simulated excess adsorption isotherms for methane (CH_4) at 20 °C in PIM-1, PIM-1c, and PIM-1n averaged over five samples are plotted along with corresponding experimental data for CH_4 in powdered PIM-1 (experimental data taken from ref 50) in Figure 7. The experimental adsorption and desorption data for PIM-1 show almost no discernible hysteresis and has therefore been reduced to just adsorption data in Figure 7 for clarity. The simulated adsorption isotherm for PIM-1, recalculated from ref 20 with corrected torsion parameters, qualitatively and quantitatively reproduces the corresponding experimental isotherm.

Adsorption isotherms for CH_4 at 20 C in PIM-1c and PIM-1n were also calculated. PIM-1c and PIM-1n represent stepwise changes in the PIM-1 functionalization of the spirocenter and backbone, respectively. The lower volume carbonyl oxygens of PIM-1c allow for closer chain packing, creating a higher density system with lower pore volume and surface area. The effect of substituting an aromatic nitrogen along the backbone in PIM-1n are less clear but create a system with slightly larger average pore sizes and surface areas than PIM-1. Despite the changes these functional modifications produced throughout the characterization, the calculated methane adsorption isotherms are nearly identical to PIM-1. The slight increase in backbone rigidity of PIM-1n compared to PIM-1, due to the aromatic nitrogen in the backbone, seems to create a more porous system. This suggests that future work should focus on increasing chain stiffness. Likewise, the volume of the spirocenter functional groups influence chain packing efficiency and may be another avenue to improve porosity and adsorption capacity.

CONCLUSIONS

In this work, a method to create physically realistic simulation samples of PIM-1 and other bifunctional PIM-1 like polymers is presented. Through a set of short MD compression and relaxation runs, realistic sample densities are achieved. The resultant sample of PIM-1 reproduces the experimentally observed X-ray scattering pattern, namely the slope and characteristic three peaks indicative of interchain spacings. Simulated scattering for PIM-1c and PIM-1n show similar characteristic peaks as PIM-1. The direct geometric probing techniques used with molecular simulations sidestep the complex models required by experiments to calculate the pore size distribution and surface areas. Given the representative and well-characterized samples, adsorption isotherms of methane in PIM-1, PIM-1c, and PIM-1n were calculated and compared to experimental data for PIM-1. The good qualitative and quantitative agreement between simulated and experimental adsorption isotherms in PIM-1 demonstrates the quality of the structure generation technique and suggests that this method can be used for other PIMs. Future work will look to explore the adsorption of polar gases (O_2, N_2, and CO_2) in these and similar polymers.

ASSOCIATED CONTENT

Supporting Information. Simulation parameters used in this work; nonbonded parameters for all atoms in all polymers are listed in Table S1; the atom identifiers for the bonded parameters are as used in GAFF and are easily associated with the atom names used throughout the rest of this work; for clarity, the atom types used along with their descriptions are given in Table S2; Tables S3−S5 list the bond, angle, and dihedral parameters, from the GAFF, used in this work; the PIM-1 structure shares many parameters with the other functional variations; parameters specific to each of the functional variations are highlighted; PIM-1c in green and PIM-1n in orange. This material is available free of charge via the Internet at http://pubs.acs.org.

AUTHOR INFORMATION

Corresponding Author
*E-mail: colina@matse.psu.edu.

ACKNOWLEDGMENT

We gratefully acknowledge funding from the Donors of the American Chemical Society Petroleum Research Fund for partial support of this research (48570-AC7) and the National Science Foundation (NSF-MWN DMR-0908781). High performance computational resources for this research were provided by the High Performance Computing Group of the Penn State ITS.

REFERENCES

(1) McNaught, A. D.; Wilkinson, A. *IUPAC Compendium of Chemical Terminology*, 2nd ed. (the "Gold Book"); Blackwell Scientific Publications: Oxford, 1997.
(2) Schüth, F.; Sing, K. S. W.; Weitkamp, J. *Handbook of Porous Solids*; Wiley-VCH: Berlin, 2002; Vols. 1−5, p 3191.
(3) Morris, R. E.; Wheatley, P. S. *Angew. Chem., Int. Ed.* **2008**, *47* (27), 4966–4981.
(4) Long, J. R.; Yaghi, O. M. *Chem. Soc. Rev.* **2009**, *38* (5), 1213–1214.
(5) Duren, T.; Bae, Y. S.; Snurr, R. Q. *Chem. Soc. Rev.* **2009**, *38* (5), 1237–1247.
(6) Duren, T.; Sarkisov, L.; Yaghi, O. M.; Snurr, R. Q. *Langmuir* **2004**, *20* (7), 2683–2689.
(7) Germain, J.; Frechet, J. M. J.; Svec, F. *Small* **2009**, *5* (10), 1098–1111.
(8) Wood, C. D.; Tan, B.; Trewin, A.; Niu, H.; Bradshaw, D.; Rosseinsky, M. J.; Khimyak, Y. Z.; Campbell, N. L.; Kirk, R.; Stockel, E.; Cooper, A. I. *Chem. Mater.* **2007**, *19* (8), 2034–2048.
(9) Abbott, L. J.; Colina, C. M. *Macromolecules* **2011**, *44* (11), 4511–4519.
(10) Tsyurupa, M. P.; Davankov, V. A. *React. Funct. Polym.* **2006**, *66* (7), 768–779.
(11) McKeown, N. B.; Budd, P. M. *Chem. Soc. Rev.* **2006**, *35* (8), 675–683.
(12) Ghanem, B. S.; Hashem, M.; Harris, K. D. M.; Msayib, K. J.; Xu, M.; Budd, P. M.; Chaukura, N.; Book, D.; Tedds, S.; Walton, A.; McKeown, N. B. *Macromolecules* **2010**, *43* (12), 5287–5294.
(13) McKeown, N. B.; Budd, P. M. *Macromolecules* **2010**, *43* (12), 5163–5176.
(14) Carta, M.; Msayib, K. J.; Budd, P. M.; McKeown, N. B. *Org. Lett.* **2008**, *10* (13), 2641–2643.
(15) Kricheldorf, H. R.; Fritsch, D.; Vakhtangishvili, L.; Lomadze, N.; Schwarz, G. *Macromolecules* **2006**, *39* (15), 4990–4998.
(16) Gelb, L. D. *MRS Bull.* **2009**, *34* (8), 592–601.
(17) Theodorou, D. N.; Suter, U. W. *Macromolecules* **1985**, *18* (7), 1467–1478.
(18) Fang, W.; Zhang, L.; Jiang, J. *Mol. Simul.* **2010**, *36* (12), 992–1003.

(19) Heuchel, M.; Fritsch, D.; Budd, P. M.; McKeown, N. B.; Hofmann, D. *J. Membr. Sci.* **2008**, *318* (1−2), 84–99.
(20) Larsen, G. S.; Lin, P.; Siperstein, F. R.; Colina, C. M. *Adsorption* **2011**, *17* (1), 21–26.
(21) McGreevy, R. L.; Pusztai, L. *Mol. Simul.* **1988**, *1* (6), 359–367.
(22) Salazar, R.; Gelb, L. D. *Langmuir* **2007**, *23* (2), 530–541.
(23) Thomson, K. T.; Gubbins, K. E. *Langmuir* **2000**, *16* (13), 5761–5773.
(24) Pikunic, J.; Clinard, C.; Cohaut, N.; Gubbins, K. E.; Guet, J. M.; Pellenq, R. J. M.; Rannou, I.; Rouzaud, J. N. *Langmuir* **2003**, *19* (20), 8565–8582.
(25) Hofmann, D.; Fritz, L.; Ulbrich, J.; Schepers, C.; Bohning, M. *Macromol. Theory Simul.* **2000**, *9* (6), 293–327.
(26) Karayiannis, N. C.; Mavrantzas, V. G.; Theodorou, D. N. *Macromolecules* **2004**, *37* (8), 2978–2995.
(27) Plimpton, S. *J. Comput. Phys.* **1995**, *117* (1), 1–19.
(28) Martin, M. G.; Siepmann, J. I. *J. Phys. Chem. B* **1998**, *102* (14), 2569–2577.
(29) Wang, J.; Wolf, R. M.; Caldwell, J. W.; Kollman, P. A.; Case, D. A. *J. Comput. Chem.* **2004**, *25* (9), 1157–1174.
(30) Cornell, W. D.; Cieplak, P.; Bayly, C. I.; Gould, I. R.; Merz, K. M.; Ferguson, D. M.; Spellmeyer, D. C.; Fox, T.; Caldwell, J. W.; Kollman, P. A. *J. Am. Chem. Soc.* **1995**, *117* (19), 5179–5197.
(31) Rai, N.; Siepmann, J. I. *J. Phys. Chem. B* **2007**, *111* (36), 10790–10799.
(32) Wick, C. D.; Stubbs, J. M.; Rai, N.; Siepmann, J. I. *J. Phys. Chem. B* **2005**, *109* (40), 18974–18982.
(33) Martin, M. G.; Siepmann, J. I. *J. Phys. Chem. B* **1999**, *103* (21), 4508–4517.
(34) Lee, J.-S.; Wick, C. D.; Stubbs, J. M.; Siepmann, J. I. *Mol. Phys.* **2005**, *103* (1), 99–104.
(35) Stubbs, J. M.; Potoff, J. J.; Siepmann, J. I. *J. Phys. Chem. B* **2004**, *108* (45), 17596–17605.
(36) Myers, A. L.; Monson, P. A. *Langmuir* **2002**, *18* (26), 10261–10273.
(37) Budd, P. M.; McKeown, N. B.; Fritsch, D. *Macromol. Symp.* **2006**, *245*−*246* (1), 403–405.
(38) Allen, M. P.; Tildesley, D. J. *Computer Simulation of Liquids*; Oxford University Press: New York, 1989.
(39) Mondello, M.; Yang, H. J.; Furuya, H.; Roe, R. J. *Macromolecules* **1994**, *27* (13), 3566–3574.
(40) Le Roux, S.; Petkov, V. *J. Appl. Crystallogr.* **2010**, *43*, 181–185.
(41) McDermott, A. G.; Larsen, G. S.; Budd, P. M.; Colina, C. M.; Runt, J. *Macromolecules* **2011**, *44* (1), 14–16.
(42) Horvath, G.; Kawazoe, K. *J. Chem. Eng. Jpn.* **1983**, *16* (6), 470–475.
(43) Pethrick, R. A. *Prog. Polym. Sci.* **1997**, *22* (1), 1–47.
(44) Gelb, L. D.; Gubbins, K. E. *Mol. Phys.* **1999**, *96* (12), 1795–1804.
(45) Frenkel, D.; Smit, B. *Understanding Molecular Simulation*; Academic Press: Orlando, FL, 2001.
(46) Duren, T.; Millange, F.; Ferey, G.; Walton, K. S.; Snurr, R. Q. *J. Phys. Chem. C* **2007**, *111* (42), 15350–15356.
(47) Budd, P. M.; Elabas, E. S.; Ghanem, B. S.; Makhseed, S.; McKeown, N. B.; Msayib, K. J.; Tattershall, C. E.; Wang, D. *Adv. Mater.* **2004**, *16* (5), 456–459.
(48) Ghanem, B. S.; McKeown, N. B.; Budd, P. M.; Fritsch, D. *Macromolecules* **2008**, *41* (5), 1640–1646.
(49) McKeown, N. B.; Budd, P. M.; Book, D. *Macromol. Rapid Commun.* **2007**, *28* (9), 995–1002.
(50) Larsen, G. S.; Siperstein, F. R.; Budd, P. M.; Colina, C. M. *Ind. Eng. Chem. Res.* **2011**.